Hindawi
International Journal of Photoenergy
Volume 2022, Article ID 4741428, 14 pages
https://doi.org/10.1155/2022/4741428

Research Article

An Artificial Neural Network-Based Comprehensive Solar Photovoltaic Emulator

Kalaimohan Thankanadar Saraswathi,[1] **Parassuram Arumugam**,[2] **Gurunandh V. Swaminathan**,[1] **and Somasundaram Periasamy**[1]

[1]*Dept. of Electrical and Electronics Engineering, CEG, Anna University, Chennai, India*
[2]*Dept. of Electrical and Electronics Engineering, Meenakshi Sundararajan Engineering College, Chennai, India*

Correspondence should be addressed to Kalaimohan Thankanadar Saraswathi; tskalaimohan12@gmail.com

Received 4 March 2022; Revised 8 April 2022; Accepted 12 April 2022; Published 11 May 2022

Academic Editor: Kumarasamy Sudhakar

With increasing solar photovoltaic-based power generation, a photovoltaic emulator (PVE) is necessary to experimentally validate new control strategies without the influence of external factors such as irradiance and temperature. However, two significant challenges with PVEs are (i) solving the nonlinear equation of photovoltaic (PV) panel and (ii) oscillations in constant current (voltage) region with voltage (current) control. Thus, in this paper, a PVE with the ability to mimic both uniformly irradiated and partially shaded PV panels is proposed by employing artificial neural network (ANN) and piecewise-linearization technique. Based on the input operating conditions (irradiance, temperature, and partial shading), the ANN breaks the nonlinear I-V curve into piecewise-linear segments and outputs their boundary points. Then, with these boundary points, piecewise-linear equations of the segments relating PVE's voltage and current are formed. Subsequently, using these piecewise-linear equations, the reference PVE voltage corresponding to PVE's output current is calculated and given to the PI controller of a synchronous buck converter to mimic a PV panel. Thus, the proposed PVE overcomes the problem of solving nonlinear I-V equation by piecewise linearization which in turn aids an impedance-matching technique to mitigate the aforementioned oscillations. The generation of training data and development of ANN were carried out in MATLAB. Finally, the simulation studies performed in MATLAB/Simulink and hardware experiments validated the steady-state accuracy and the transient response which settled within 10 ms endorsing the real-time application of the proposed PVE.

1. Introduction

The alarming consequences of global warming have forced the world's electricity systems to "decentralize, decarbonize, and democratize", in many cases from the bottom up [1]. With increasing awareness of the environmental issues, the application of renewable energy in power systems has become the need of the day to decarbonize the power sector [2, 3]. The penetration of renewable energy sources (RESs) in power system generation has significantly increased; microgrids have been employed as an effective way to tackle the challenges associated with the intermittent nature of renewable sources and load, as load demands are satisfied locally through distributed generators (DGs) (decentralized approach) [4, 5].

Solar power is one of the renewable sources that is widely researched around the world as a viable source in microgrid system [6]. Power generated by solar photovoltaic (PV) panels depends on solar irradiance and temperature which vary continuously due to changing weather conditions. Therefore, solar PV-based power generation introduces challenges such as power quality degradation, stability issues, and reliability concerns [7]. To improve the performance of solar PV panels, different power management strategies are to be explored and experimented with. However, to study the behavior of solar PV system with new power management strategies, the solar PV panel should be operated in a controlled irradiance and temperature condition which is difficult to achieve practically. This led to the development of solar PV emulator (PVE) which mimics the

behavior of an actual solar PV panel. Over several years, researchers have developed different models of PVEs and the most common type of PVE is the standard PVE developed using I-V characteristics of PV cells [8].

In [9], the authors have proposed a PVE using buck converter and dSPACE controller in which PV model is implemented in MATLAB/Simulink. The PV model takes PV current as input and PV voltage as output which is then tracked using a PI controller. However, this method requires a dSPACE controller which is not cost-effective, and also, the nonlinear governing equation of the PV panel needs to be solved which can be time-consuming. In [10], the authors have developed a PVE employing buck converter with PV model implemented in an FPGA through Matlab/XSG toolbox. The model takes irradiance, temperature, and PV voltage as input and computes PV current as output to be tracked by a buck converter's PI controller. However, the problem of solving the nonlinear I-V equation is not addressed. Authors of [8] have provided an exhaustive review on PVEs where the existing PVEs are compared based on factors, such as complexity, accuracy, implementation methodology, and hardware implementation, and addressed the complexity associated with emulating a PV panel under partially shaded conditions. In [11], the authors have proposed a resistance feedback controller and have modified the single diode model of PV into the current-resistance (I-R) model which is solved using the binary search method. The model gives PV current as output which is then regulated using a buck converter. A PVE employing fractional order sliding mode controller governed by two-diode model for PV panel is proposed in [12] where the two diode model increases the PVE's accuracy with the fractional order sliding mode controller ensuring the robust operation of the PVE against load changes and other disturbances.

The role of artificial neural network (ANN) in the field of solar PV generation is explored extensively in [13–16]. In [13], the authors have developed an ANN model to predict the output power of PV panels. The ANN model takes irradiance and temperature as inputs and gives I-V characteristics as output. Gradient Descent Least Squares Regression-based ANN is proposed in [14] that extracts the fundamental component of current in a grid-connected solar PV system for its control while improving power quality. Whereas [15] employs a steepest descent laplacian regression for a single-layer ANN that control a grid-supporting solar PV system. The single-layer ANN of [14, 15] decreases the computation time while making the controller robust against abnormal grid conditions. The authors of [16] have developed an ANN with two hidden layers with irradiance, temperature as input, and panel power as output. Further evolutionary programming has been used to train and optimize the neural architecture. In [17], the authors have implemented an ANFIS for emulating and analyzing the characteristics of PV panels in real-time using FPGA and also suggested that both ANN and ANFIS can be utilized in the developed PVE in terms of accuracy. However, in terms of response speed, ANN was significantly slower. To meet the active power requirement of loads in a grid-connected PV system, a leaky least logarithmic absolute difference-based ANN is proposed in [18] along with a novel learning-based incremental conductance maximum power point tracking (MPPT) algorithm, whereas in [19], a novel Perturb and Observe MPPT algorithm and Leaky Least Mean Logarithmic Fourth learning method for a single layer ANN to control active power of a grid-connected PV system is proposed. In [20], power normalized kernel least mean fourth-based ANN is proposed for active load component extraction from a distorted load current thereby attenuating harmonics, DC bias and other distortions The authors of [21] have proposed PVE employing a PI-controlled two-stage interleaved buck converter with a two-stage LC filter and single diode model for solar PV. To have a fast response, the controller gains are varied as a function of the PVE's output resistance and irradiance. The functions mapping input irradiance and resistance to PI gains are determined using an ANN. A look-up table-based PVE, proposed in [22], takes PV current as input and gives PV voltage as output. The output PV voltage is given as a reference to a DC-DC converter controlled by a sliding mode controller. However, relying on a look-up table has limited the PVE's range of operating temperature and irradiance. Authors of [23] have proposed an efficiency enhancement technique for current source-diode string-based PVE where the diode string is swapped with a noninverting buck-boost converter when the PVE operates near the open-circuit voltage region. An impedance-matching technique is proposed in [24] to overcome the problem of oscillating voltage (current) reference signal when a PVE operates in a constant current (voltage) region. However, a look-up table is employed to model a PV panel which not only limits the operating range of the PVE but also necessitates an integral controller for impedance matching.

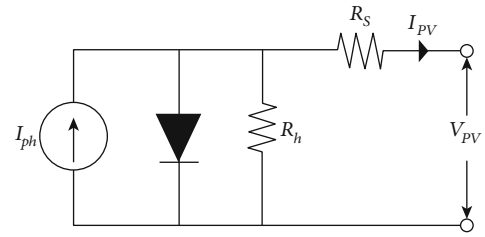

Figure 1: Equivalent circuit of PV panel.

Based on the above-cited research works, the major challenge lies in solving the nonlinear equation governing the PV panel quickly while mitigating the oscillations in constant current/voltage region with voltage/current control. The research works cited above use a high-end computational device [9, 10, 17] which increases the cost of the system, whereas other research works employ an ANN-based technique to fit the entire nonlinear I-V characteristics [13, 16, 17]. Thus, the ANN has to be executed continuously to determine the controller's reference signal (V_{PV}/I_{PV}) for load changes which is not effective as the computational time may get increased depending on the size of the ANN. Meanwhile other research works adopt a look-up table to mimic

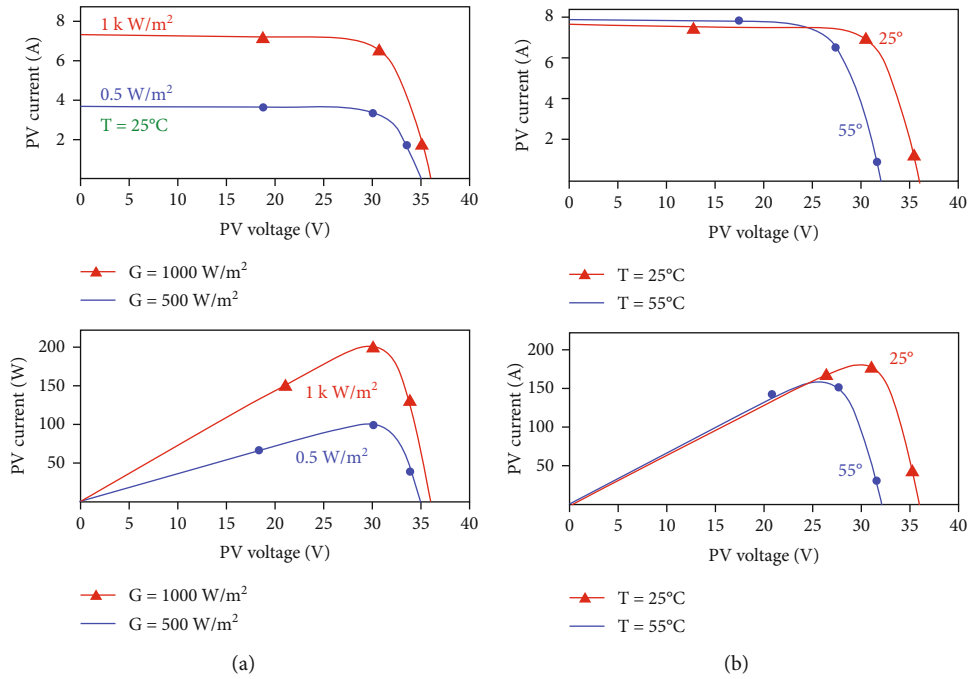

Figure 2: I-V and P-V characteristics of a PV panel. (a) Irradiance change. (b) Temperature change.

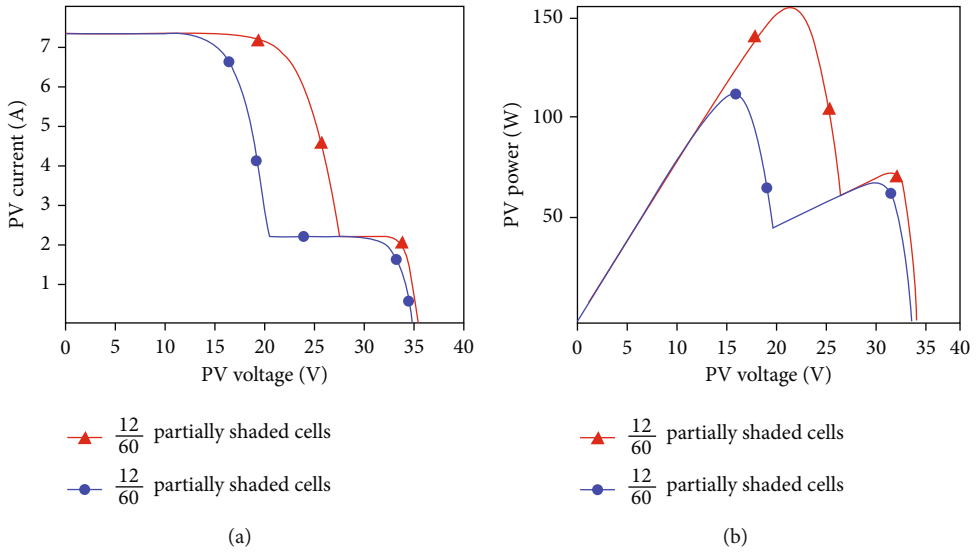

Figure 3: Partially shaded PV panel. (a) I-V curve. (b) P-V curve.

the I-V characteristic curve [22] which can get tedious with more number of unique I-V characteristic curves for every combination of temperature and irradiance. Thus, to address this research gap, inspired by the piecewise linear model of diode [25], the authors of this paper propose a PVE based on a piecewise-linearized I-V curve. The I-V curve is divided into small, linear segments with clearly defined intervals (end points). These intervals define the boundary conditions of the individual linear segments in the piecewise-linear function and are predicted using a pretrained ANN. Using the piecewise linear function formed with the predicted boundary conditions, panel voltage is calculated for a particular current which is then given as a reference to control a synchronous buck converter whose output terminals mimic the behavior of an actual PV panel. Thus, the major contributions of the paper are

(1) A PVE based on a piecewise-linearized I-V curve is proposed which drastically decreases the computational time and computational power requirement

(2) An ANN is employed to compute the boundary conditions of the piecewise-linear equation based on temperature and irradiance. This enables the pro-

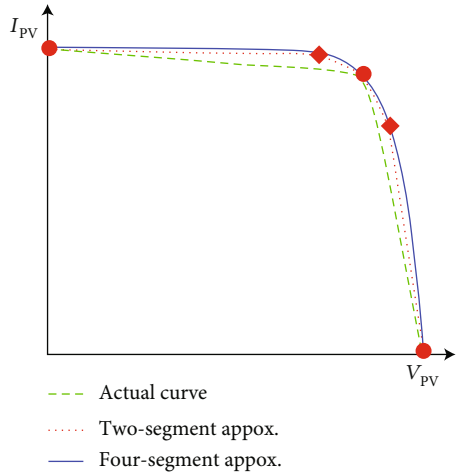

Figure 4: Piecewise linearization of I-V curve.

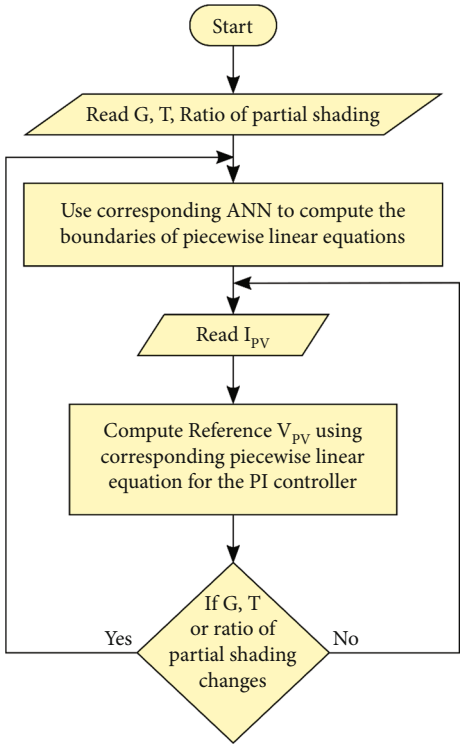

Figure 5: Flowchart of the proposed PVE.

posed PVE to operate over a wide range of temperature and irradiance variations

(3) Then, the proposed PVE is expanded to include the effect of commonly-encountered partial shading condition and hence the ANN takes an additional input representing the ratio of panel receiving reduced irradiance

(4) Furthermore, the problem of voltage reference oscillation in constant current region operation is overcome by the impedance matching method without any additional controller

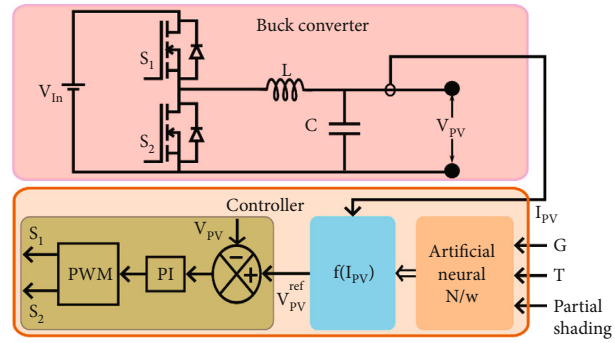

Figure 6: Block diagram of the proposed ANN-based PVE.

The structure of the paper is as follows. Section 2 discusses the modeling of solar PV panels and their I-V, P-V characteristics. Section 3 explains the design of the proposed solar PVE along with the impedance matching method for mitigating the oscillatory reference signal. Section 4 contains simulation results along with relevant discussion. Section 5 contains hardware setup with experimental validation. Finally, Section 6 concludes the paper.

2. Modeling and Characteristics of Solar PV Panel

2.1. Modeling of Solar PV Panel. Since the objective is to mimic the behavior of a PV panel, it is essential to develop its mathematical model to generate the data for training the ANN. The developed mathematical model also serves as a benchmark for evaluating the performance of the proposed PVE measured using root mean square error (RMSE). The equivalent circuit diagram of a solar PV panel based on the single diode model is shown in Figure 1.

The output current of a PV panel is given by equation (1) [26, 27].

$$I_{PV} = N_P I_{ph} - N_P I_o \left(\exp\left[\frac{q\left(V_{PV}/N_s + I_{PV}R_s/N_p\right)}{nkT} \right] - 1 \right) - \frac{V_{PV} + I_{PV}R_s}{R_h}, \quad (1)$$

where R_h and R_s are the shunt and series resistance, respectively; $V_{PV}, I_o, I_{ph}, I_{PV}$ are the PV panel output voltage, diode reverse saturation current, light generated current, and PV panel output current, respectively. N_p and N_s are the number of parallel and series-connected cells, respectively. n, k, T, and q are diode ideality factor ($1 < n < 2$, $n = 1$ for ideal diode), Boltzmann's constant (1.38×10^{-23} J/K), the temperature of PV panel, and charge of an electron ($1.6 \times 10^{-19^\circ}$C), respectively.

The temperature of the PV panel affects the diode reverse saturation current (I_o) and the light generated current (I_{ph}), whereas the irradiance (G) affects only the light generated current. Thus, the effect of temperature on the reverse saturation current is given by equation (2) whereas equation (3) relates temperature and irradiance with the

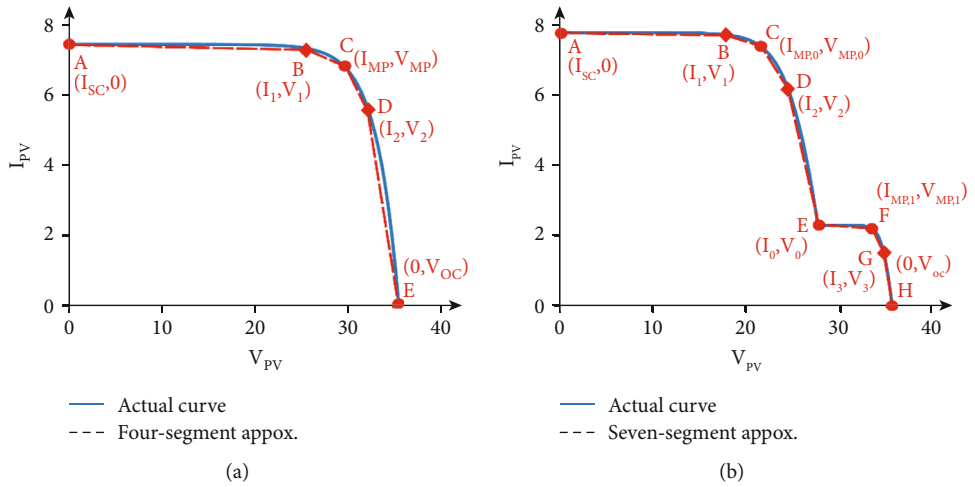

FIGURE 7: Piecewise linearization of I-V curves of (a) uniformly irradiated (b) partially shaded PV panel.

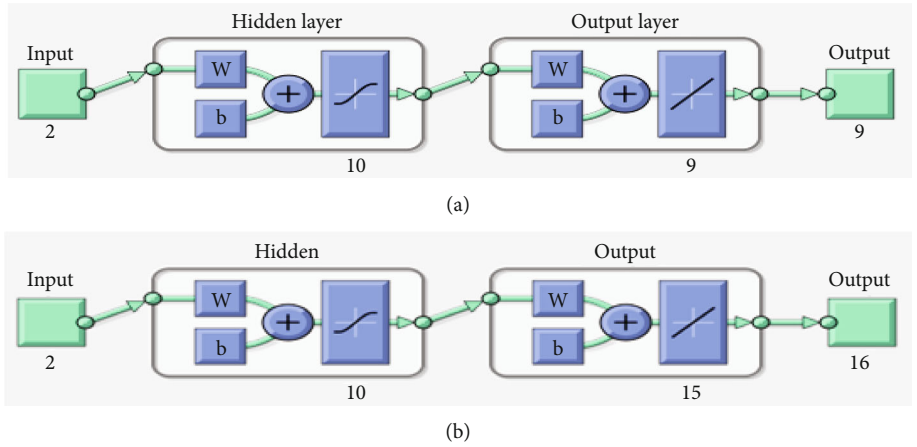

FIGURE 8: Structure of ANN for PVE under (a) uniformly irradiated (b) partially shaded conditions.

light generated current [27]. For more information on PV array modelling, the readers are referred to [27]

$$I_o = I_{o,n}\left(\frac{T_n}{T}\right)^3 \exp\left(\frac{qE_{g0}}{nk}\left(\frac{1}{T_n} - \frac{1}{T}\right)\right), \quad (2)$$

$$I_{ph} = \left(I_{ph,n} + K_1(T - T_n)\right)\frac{G}{G_n}, \quad (3)$$

where $T_n, G_n, I_{o,n}, I_{ph,n}, E_{g0}, K_1$ is the nominal temperature (25°C), nominal irradiance (1000 W/m^2), nominal saturation current, nominal light generated current, bandgap energy of solar cell, and temperature coefficient for short circuit current, respectively.

2.2. Characteristics of Solar PV Panel. Three significant inferences that can be drawn from equations (1)-(3) are (i) the nonlinear relationship between I_{PV} and V_{PV}, and (ii) the nonlinearity in the relationship can be attributed to the diode present in the equivalent circuit (iii) the influence of temperature and irradiance (and hence shading conditions as well) on the I-V characteristics of a solar cell. To understand the impact of temperature and irradiance, I-V and P-V characteristics are simulated for two different irradiance values and temperatures with one parameter kept constant at its STC value while the other parameter is varied.

With the temperature fixed at 25°C, I-V and P-V characteristics are simulated for irradiance values of 500 W/m^2 and 1000 W/m^2 as shown in Figure 2(a) which reveals that the short circuit current varies linearly with irradiance, whereas open-circuit voltage has nonlinear relation with irradiance. Thus, as a result, maximum power has an approximately linear dependence on irradiance.

For a fixed irradiance of 1000 W/m^2, I-V and P-V curves for a temperature of 25°C and 55°C are obtained as shown in Figure 2(b). It can be inferred from Figure 2(b) that the open-circuit voltage is more sensitive to change in temperature whereas short circuit current varies only by a small amount which makes maximum power vary nonlinearly with respect to temperature.

Solar PV panels operating under nonuniform irradiance due to partial shading caused by passing clouds, trees, bird droppings, building structures are not uncommon [28]. Partial shading can cause severe performance degradation

Results

	Sample	MSE	R
Training:	205	2.57477e-2	9.99995e-1
Validation:	68	3.59584e-2	9.99993e-1
Testing:	68	3.41452e-2	9.99993e-1

(a)

Results

	Sample	MSE	R
Training:	93	2.09774e-3	9.99995e-1
Validation:	31	2.24696e-3	9.99993e-1
Testing:	31	1.33831e-3	9.99993e-1

(b)

Figure 9: Summary of ANN training.

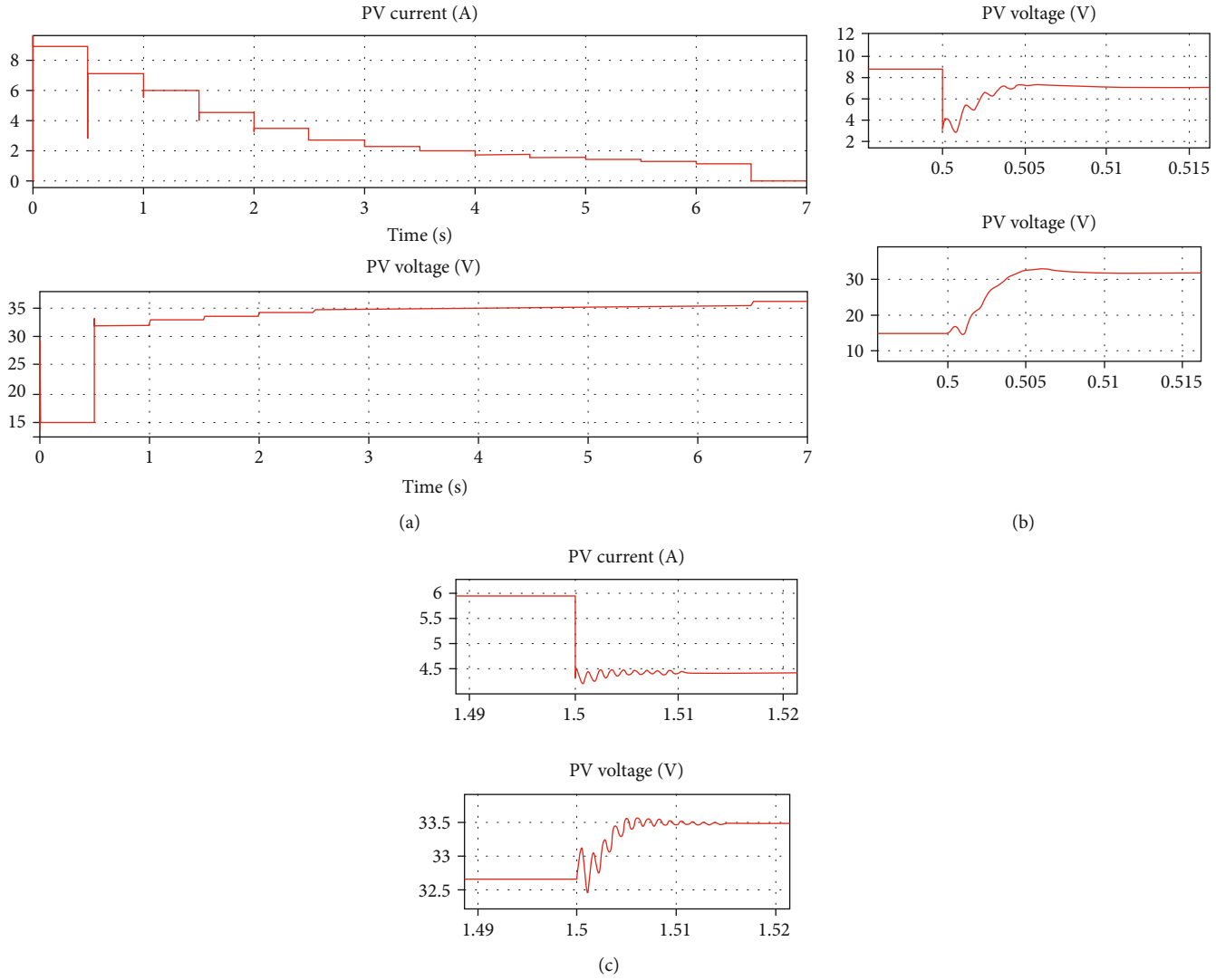

Figure 10: PVE current and voltage under uniform irradiance condition for load change case. (a) Entire curve. (b) Transient response at $t = 0.5$ s. (c) Transient response at $t = 1.5$ s.

calling for additional efforts such as bypass diodes to mitigate its detrimental impacts, and hence, power management strategies capable of handling partial-shading conditions as well are desired. Motivated by this, the proposed PVE is designed to mimic a PV panel receiving two different irradiances across its entire area. To study the characteristics of a partially shaded PV panel, the temperature is maintained at 25°C, unshaded cells are given an irradiance of 1000 W/m^2 whereas shaded cells are given 300 W/m^2 irradiance and I-V, and P-V characteristics are obtained with 12 and 24 cells (out of 60) of the panel receiving reduced irradiance. Figure 3 shows the corresponding family of I-V and P-V

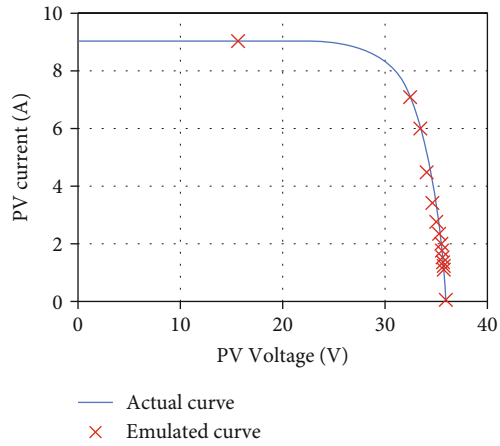

Figure 11: I-V characteristics for uniform irradiance condition.

characteristics which reveals that there is one global and one local maximum in P-V characteristics. Another interesting observation is that the number of maxima points in the P-V curve is equal to the number of regions on the PV panel that are receiving different irradiance.

3. Design of the Proposed PV Emulator

As mentioned earlier, two major challenges in a PVE are (i) solving the nonlinear equation governing the panel and (ii) oscillatory reference signal in constant current (voltage) region with voltage (current) control mode. To overcome the issue of solving the nonlinear equation, the authors of this paper propose to split the nonlinear I-V curve into small, linear segments thereby reproducing the entire nonlinear curve with a piecewise linear function defined by a linear equation for each segment. Evidently, with more segments, the accuracy of the piecewise-linear model is improved which can be inferred from Figure 4 containing two-segment and four-segment piecewise linear models.

The other issue of the oscillatory reference signal can be overcome by the impedance matching method. [24] As can be inferred from the I-V characteristics, voltage is extremely sensitive to current in the constant current region whereas the current is extremely sensitive to voltage in the constant voltage region of the I-V curve. Thus, when the voltage control mode is employed in the constant current region, a small ripple in current shall result in large oscillations in the reference voltage signal, whereas with current control mode in constant voltage region, a small noise in voltage signal shall induce oscillations in reference current signal. This issue is overcome with an additional integral controller trying to match the load impedance with that of PVE in ref. [24]. This is because the stable, equilibrium operating point of a PVE is the intersection of I-V characteristics of the PVE with that of the load. Since the proposed PVE typically employs a linear approximation, the intersection of the load and PVE characteristics can be calculated in a single step without any additional integral controller. Thus, both the major challenges are overcome by adopting a piecewise-linear model for a PV panel.

Consequently, given a particular I-V curve for certain irradiance, temperature, and ratio of partial shading, its corresponding piecewise-linear model depends on the boundary conditions which are strongly coupled with the aforementioned operating conditions. Hence, an ANN model is employed to predict the boundary conditions for a given set of operating conditions. This enables the proposed PVE to operate over a wide range of operating conditions. Finally, the piecewise linear function takes PV current as input to compute the corresponding PV voltage which is then tracked by a PI controller controlling a synchronous buck converter. The flowchart of the proposed PVE and its overall block diagram are shown in Figures 5 and 6, respectively. Thus, the design of the proposed PVE can be split into three phases as (i) ANN model, (ii) deriving an expression for each segment in piecewise linear function, and (iii) design and development of synchronous buck converter.

3.1. ANN Model. A PVE should have the ability to mimic PV panels under a wide range of operating conditions, namely, temperature, irradiance, and the ratio of partial shading. However, the boundary conditions of each segment in the piecewise linear function vary with the aforementioned operating conditions. Hence, logic is required to determine the corresponding boundary conditions and an ANN is a good solution to this because of its ability to represent nonlinear equations through regression. The neural network toolbox available in MATLAB is used in this study. Hence, in this regression problem, the input variables (features or independent variables) are (i) temperature, (ii) irradiance, and (iii) ratio of partial shading, whereas the output variables (dependent variables) are the Cartesian coordinates of the boundary conditions (I_{PV}, V_{PV} of corresponding segment boundaries) along with the peak powers. The peak power is also added as an output variable so that the ANN model can be tested more effectively. Based on this schema, training data must be generated since the performance of ANN depends on how well the network is trained. Before generating the training data, it is essential to decide upon the number of segments for linearizing the I-V curve.

Based on visual observation, the uniform-irradiance and partial-shading I-V curves are split into 4 and 7 segments, respectively, as shown in Figures 7(a) and 7(b), respectively. Thus, for the uniform-irradiance I-V curve (Figure 7(a)), the output variables are peak power and the five points from A to E which are defined by [I_{PV}, V_{PV}] in the Cartesian coordinates. Since the points from A to E have two values each (I_{PV}, V_{PV}), there are 10 (5×2) values along with 1 peak power as output variables. However, for point A (short circuit) $V_{PV,A} = 0$, and for point E (open circuit), $I_{PV,E} = 0$. Hence, those two values can be ignored which makes the total number of output variables = 9 (10 values for points A-E+1 for peak power−2 for $V_{PV,A}, I_{PV,E}$). Similarly, for the partial-shading I-V curve, 8 points from A to H along with two peak powers are the dependent variables leading to a total of 16 output variables.

After finalizing the data schema, training data were generated by varying the temperature from 20°C to 50°C for every value of irradiance ranging from 500 W/m^2 to 1000 W/m^2 in steps of 50 W/m^2 for uniform irradiance condition. However, for the partial-shading condition, the number of independent factors affecting the performance is (i) temperature, (ii) number of regions of the panel receiving different irradiances (=number of peaks in the P-V curve), (iii) area of such regions receiving different irradiances (=number of cells in such regions), and (iv) irradiance values for those regions. For brevity, the number of regions receiving different irradiances was fixed at two and their irradiances were fixed at 300 W/m^2 and 1000 W/m^2. The areas of these two regions were obtained from the user as ratio of the panel receiving reduced irradiance. Thus, for training-data generation, the panel temperature was varied from 20°C to 50°C for a ratio of partial shading ranging from 0.1 to 0.5 in steps of 0.1. Thus, a total of 341 and 155 observations were generated as per the aforementioned schema for uniform irradiance and partial-shading conditions, respectively, to train the corresponding networks. The generated dataset is hosted publicly in Mendeley Data and can be accessed at [29].

Since the number of dependent variables (output variables) varies for uniform irradiance and partial-shading conditions, the proposed PVE employs two separate ANN models as shown in Figures 8(a) and (b), respectively. In case of uniform-irradiance conditions, the inputs are temperature and irradiance, whereas for partial-shading conditions, the inputs are temperature and ratio of partial shading.

One interesting observation from Figure 8(b) is the difference in the number of outputs (16) and the number of neurons in the output layer (15). This is because of the way the data was generated. As mentioned earlier, during data generation for partial-shading conditions, the irradiance level for shaded cells was fixed at 300 W/m^2 and the 155 observations were generated by varying the operating temperature from 20°C to 50°C and partial shading conditions ranging from 0.1 to 0.5. However, the current I_o at E in Figure 7(b) depends only on the irradiance of shaded cells (which was maintained constant at 300 W/m^2). Hence, I_o, an output variable, remains constant for all the 155 observations for which a separate neuron is not needed in the output layer. With the generated data, the Levenberg-Marquardt algorithm available in the neural network toolbox is employed for training, during which the number of neurons in the hidden layer was set at 10, 20, and 50 to observe mean square error (MSE). However, the MSE did not significantly improve with a higher number of neurons in the hidden layer and hence it was fixed at 10 for both models. The split-up of data for training, validation, and testing and the performance (MSE) of the models are shown in Figures 9(a) and (b) for uniform irradiance and partial-shading conditions, respectively.

3.2. Piecewise Linear Function. After developing the ANN models, the output boundary conditions are used to define the piecewise linear function describing each segment through a linear equation. The linear equation of each segment takes the PV current as input to compute the corresponding PV voltage and is of the form $V_{PV} = m_i I_{PV} + c_i$, where m_i and c_i are the slope and the intercept of the i^{th} linear segment. The piecewise linear functions for uniform irradiance and partial-shading conditions are given by equations (4) and (6), respectively. The corresponding m_i and c_i can be calculated using the two-point form of a straight line as given in equations (5) and (7), for uniform-irradiance and partial-shading conditions, respectively, where the constants (V_x, I_x) in equations (5) and (7) are the output variables from the ANN model and their positions on the I-V curve are shown in Figure 7.

As mentioned earlier, when the PVE is operating near the short circuit region, i.e., constant current region, the reference voltage has to be generated based on the impedance matching principle. Hence, in equations (4) and (6), the function definition for the constant-current region is different which can be calculated by substituting the load characteristics ($I_{PV} = V_{PV}/R_L$; where R_L is load resistance) in the corresponding PVE characteristics (-
$V_{PV} = m_1 I_{PV} + c_1 \Rightarrow V_{PV} = m_1 V_{PV}/R_L + c_1 \Rightarrow V_{PV}(R_L - m_1) = c_1 R_L$).

$$V_{PV}(I_{PV}) = \begin{cases} \dfrac{c_1 R_L}{R_L - m_1} ; I_{PV} \in [I_1, I_{SC}] \\ m_2 I_{PV} + c_2 ; I_{PV} \in [I_{MP}, I_1] \\ m_3 I_{PV} + c_3 ; I_{PV} \in [I_2, I_{MP}] \\ m_4 I_{PV} + c_4 ; I_{PV} \in [0, I_2] \end{cases}, \tag{4}$$

where

$$m_1 = \frac{V_1}{I_1 - I_{SC}} ; m_2 = \frac{V_{MP} - V_1}{I_{MP} - I_1} ; m_3 = \frac{V_2 - V_{MP}}{I_2 - I_{MP}} ; m_4 = \frac{V_2 - V_{OC}}{I_2} ;$$

$$c_1 = -m_1 I_{SC} ; c_2 = V_{MP} - m_2 I_{MP} ; c_3 = V_{MP} - m_3 I_{MP} ; c_4 = V_{OC}, \tag{5}$$

$$V_{PV}(I_{PV}) = \begin{cases} \dfrac{c_1 R_L}{R_L - m_1} ; I_{PV} \in [I_1, I_{SC}] \\ m_2 I_{PV} + c_2 ; I_{PV} \in [I_{MP,0}, I_1] \\ m_3 I_{PV} + c_3 ; I_{PV} \in [I_2, I_{MP,0}] \\ m_4 I_{PV} + c_4 ; I_{PV} \in [I_0, I_2] \\ \dfrac{c_5 R_L}{R_L - m_5} ; I_{PV} \in [I_{MP,1}, I_0] \\ m_6 I_{PV} + c_6 ; I_{PV} \in [I_3, I_{MP,1}] \\ m_7 I_{PV} + c_7 ; I_{PV} \in [0, I_3] \end{cases}, \tag{6}$$

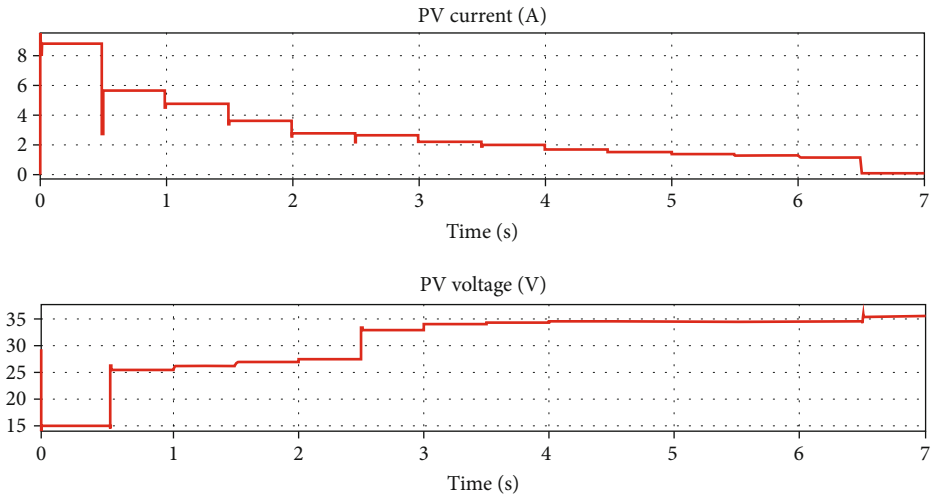

Figure 12: PVE current and voltage under 20% partially-shaded condition.

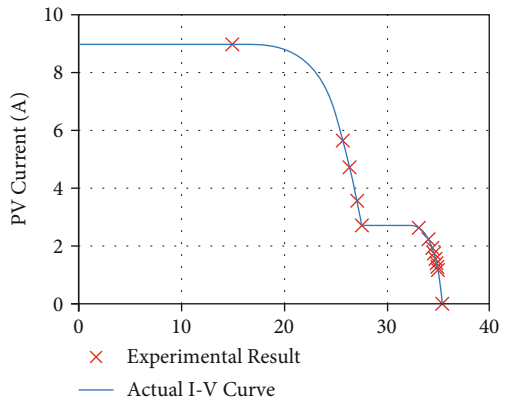

Figure 13: I-V characteristics for 20% partial shading.

where

$$m_1 = \frac{V_1}{I_1 - I_{SC}}\,;\, m_2 = \frac{V_{MP,0} - V_1}{I_{MP,0} - I_1}\,;\, m_3 = \frac{V_2 - V_{MP,0}}{I_2 - I_{MP,0}}\,;\, m_4 = \frac{V_0 - V_2}{I_0 - I_2}\,;$$
$$m_5 = \frac{V_{MP,1} - V_0}{I_{MP,1} - I_0}\,;\, m_6 = \frac{V_3 - V_{MP,1}}{I_3 - I_{MP,1}}\,;\, m_7 = \frac{V_3 - V_{OC}}{I_3}\,;$$

$$c_1 = -m_1 I_{SC}\,;\, c_2 = V_{MP,0} - m_2 I_{MP,0}\,;\, c_3 = V_{MP,0} - m_3 I_{MP,0}\,;\, c_4 = V_0 - m_4 I_0$$

$$c_5 = V_{MP,1} - m_5 I_{MP,1}\,;\, c_6 = V_{MP,1} - m_6 I_{MP,1}\,;\, c_7 = V_{OC}. \quad (7)$$

3.3. Power Converter of PVE. The output PV voltage from the piecewise linear function is given as a reference to the control loop of a DC-DC power converter which is a synchronous buck converter in this paper. The basic circuit diagram of a synchronous buck converter is depicted in Figure 6. The power converter stage can be further split into two subsections as (i) converter design stage and (ii) controller design stage.

3.3.1. Design of Power Converter. To filter out the current and voltage ripples optimally, the inductor and capacitor of the synchronous buck converter should be sized properly. Even though large values of inductor and capacitor can significantly improve ripple attenuation, the settling time of the converter increases for higher values which is not desirable for PVE. Hence, a trade-off is made between ripple attenuation and settling time and the values of inductor and capacitor can be calculated using equations (8)-(11) [30].

$$\Delta I_L = 0.3\text{x}\mathrm{I}^{\text{Rated}}, \quad (8)$$

$$L_{\min} = \frac{(V_{\text{in}} - V_{\text{out}})\text{x}D}{\Delta I_L \text{x} f_s}, \quad (9)$$

$$\Delta V_C = 0.05\text{x}V_{\text{out}}, \quad (10)$$

$$C_{\min} = \frac{\Delta I_L}{8\Delta V_C f_s}, \quad (11)$$

where ΔI_L, I^{Rated}, $L_{\min}$, V_{in}, V_{out}, D, f_s, ΔV_C, and $C_{\min}$ are the synchronous buck converter's inductor current ripple (A), rated input current (A), minimum value of inductor (H), nominal input, output voltages (V), nominal duty, switching frequency (Hz), output voltage ripple (V), and minimum value of output capacitor (F).

3.3.2. Small-Signal Model of Converter. To tune the PI controller for tracking the reference voltage from piecewise linear function, a mathematical model of the converter is necessary. Due to the nonlinear nature of the converter, a linear small-signal averaging model is derived around a quiescent operating point and the corresponding small-signal averaging model of the converter is given by equation (12) [31]. Using MATLAB's in-built PID tuning application, the PI controller is tuned by the Ziegler-Nichols method.

$$\frac{\widehat{V}}{\widehat{d}} = \frac{V_{\text{out}}/D}{1 + s(L/R) + s^2(LC)}, \quad (12)$$

where $\widehat{V}, \widehat{d}$ are the small-signal change in output voltage and duty, respectively, V_{out} is the nominal Q-point output voltage of the synchronous buck converter, D is the corresponding Q-point duty, L and C are the inductor and output

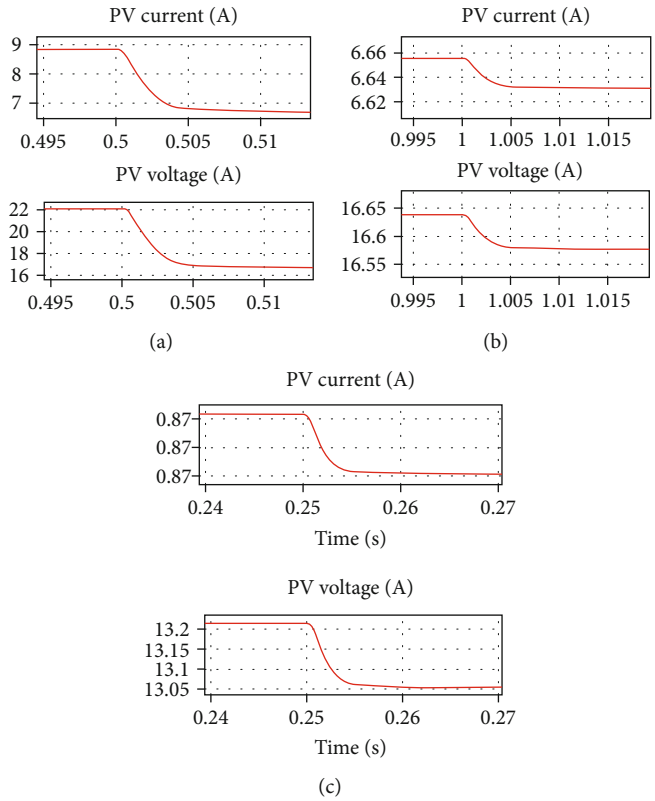

Figure 14: Transient response for changes in (a) irradiance, (b) temperature, and (c) ratio of partial shading.

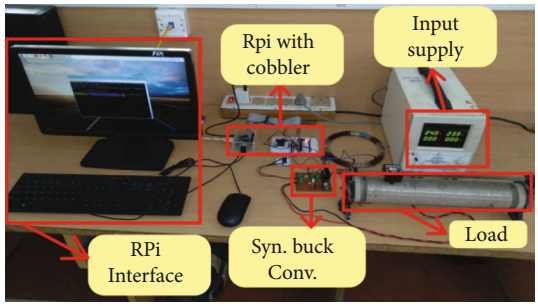

Figure 15: Experimental setup of PVE.

capacitor of the synchronous buck converter, respectively, and R is the load resistance.

4. Simulation Results and Discussion

To validate the proposed PVE, simulation studies were carried out in MATLAB/Simulink where the proposed PVE shown in Figure 6 is implemented. The ANN developed in MATLAB's neural network toolbox is also imported into the Simulink environment. Based on the timescale, the proposed PVE is assessed by its steady-state and transient performance. Good steady-state performance means a good agreement of the emulated I-V characteristics with the actual I-V characteristics, whereas a good transient response means having a quick settling time with minimal overshoot and oscillations. The PVE enters a transient state for the following conditions (i) load change, (ii) irradiance change, (iii) temperature change, and (iv) change in the ratio of partial shading.

Thus, by appropriate load switching, the steady-state performance (I-V characteristics) and transient performance for load change can be analyzed, whereas the transient performance for change in irradiance, temperature, and ratio of partial shading can be analyzed by simulating the same with load fixed at a particular value. Therefore, the simulation analysis is split into three cases. Case 1 deals with load switching for uniformly irradiated conditions whereas Case 2 again deals with load switching but for partially-shaded conditions. Finally, Case 3 deals with transient performance analysis for change in irradiance, temperature, and ratio of partial shading.

Case 1. With the temperature, irradiance, and partial shading kept at 25°C, 1000 W/m^{2,} and 0.0, respectively, and a resistive load was switched in 14 steps in a 0.5-second interval as [1.7, 4.5, 5.5, 7.5, 10, 12.5, 15, 17.5, 20, 22.5, 25, 27.5, 30, 500] Ω. Figure 10(a) shows the corresponding PVE output current and voltage. The transient responses for the load changes at time $t = 0.5$ s and at time $t = 1.5$ s are shown in Figures 10(b) and 10(c), respectively. The transient responses in Figures 10(b) and 10(c) are oscillatory, yet the

Table 1: Hardware parameters.

Parameter	Value
V_{in}	48 V
Switching frequency	20 kHz
Inductor, L	140 μH
Output capacitor, C	220 μF
PI controller $[K_p, K_i]$	[0.0022, 4.2157]

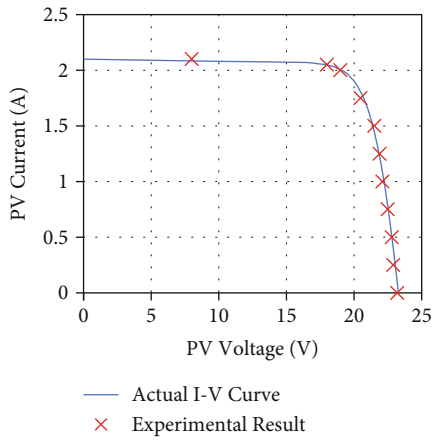

Figure 16: I-V characteristics obtained from experimental setup of PVE.

system reaches steady-state in around 10 ms duration which is a good value [24] because neither advanced nor additional controllers are employed in this work. Meanwhile, Figure 11 shows that the emulated I-V curve is in good agreement with the reference I-V curve. Thus, the steady-state performance under uniformly irradiated condition and the transient performance of the proposed PVE for load change are satisfactory.

Case 2. Similar to Case 1, with irradiance and temperature fixed at 1000 W/m^2 and 25°C, respectively, the load resistance was switched in steps with a 0.5-second interval as [1.7, 4.5, 5.5, 7.5, 10, 12.5, 15, 17.5, 20, 22.5, 25, 27.5, 30, 500] Ω. But in this case, the ratio of partial shading is fixed at 0.2 (20% of the panel is partially illuminated). Figure 12 shows the corresponding PVE output current and voltage where the transient response during load change was similar to that in Case 1 (and hence not shown separately). Meanwhile, Figure 13 shows that the corresponding I-V curve of the proposed PVE is in good agreement with the reference I-V curve validating its steady-state performance under partially-shaded condition.

Case 3. This case deals with the analysis of the proposed PVE's transient performance for irradiance change and temperature change under uniformly irradiated conditions. Furthermore, the proposed PVE's transient performance for a

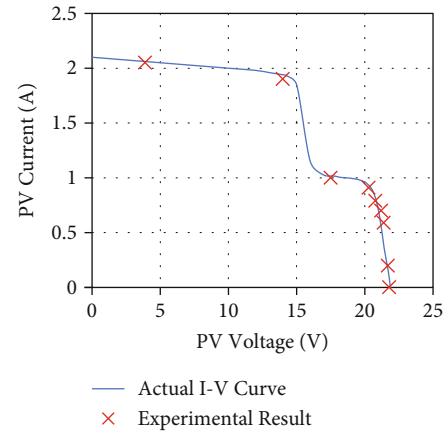

Figure 17: I-V characteristics obtained from the experiment.

change in the ratio of partial shading while operating under partially shaded conditions is also analyzed. The load resistance is fixed at 2.5 Ω thereby ensuring that the PVE is operated in the constant-current region.

Figure 14(a) shows the transient response of the PVE at 25°C when its irradiance is changed from 1000 W/m^2 to 750 W/m^2. The transient profile is smooth with a settling time of less than 7.5 ms for the aforementioned irradiance change. Then, with irradiance fixed at 750 W/m^2, the temperature is changed from 25°C to 30°C producing a smooth transience to the new steady state settling within 5 ms as shown in Figure 14(b). Finally, with the irradiance, and temperature fixed at 1000 W/m^{2,} and 25°C, the ratio of partial shading was changed from 0.2 to 0.3 resulting in a smooth decrease in voltage and current as shown in Figure 14(c). It can be noted that there is a small delay during the beginning of transience which is caused by the ANN while computing the new boundary conditions for the piecewise-linear function. However, the total settling time is within 10 ms for all the cases along with a smooth transient profile.

From the simulation results, it is clear that the proposed PVE has a good steady-state as well as a good transient performance with a quick settling time of around 10 ms for changes in load, irradiance, temperature, and ratio of partial shading. This proves that the proposed PVE has successfully overcome the problem of solving the nonlinear equation by piecewise linearization. Furthermore, the simulation results also prove that the proposed PVE has overcome the problem of reference oscillations in constant current/voltage region without any additional controller.

5. Experimental Verification

A laboratory-scale hardware setup is implemented to validate the proposed PVE. The block diagrams shown in Figure 6 containing ANN model, piecewise linear function, and PI controller are implemented using Raspberry Pi (RPi) and the experimental setup is shown in Figure 15. Table 1 shows the specifications for hardware components used in the DC-DC converter.

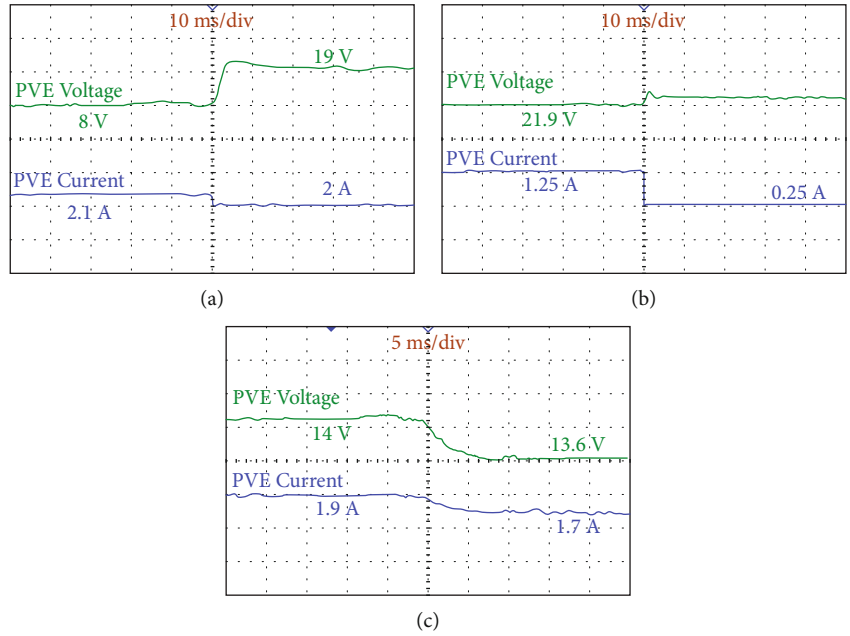

Figure 18: Transient performance of the proposed PVE for load change near (a) constant current, (b) constant voltage regions, and (c) for change in ratio of partial shading.

Two main objectives of the experimental verification are validating (i) the steady-state accuracy and (ii) the transient performance of the proposed PVE. Thus, to verify the steady-state accuracy, irradiance and temperature are set at 1000 W/m^2 and 25°C, respectively, and the load is varied to obtain the I-V characteristics shown in Figures 16 and 17 for uniform irradiance and partially shaded condition with the ratio of partial shading set to 0.2, respectively. Figures 16 and 17 show that the experimentally observed values are in good agreement with the actual I-V curves thereby validating the steady-state accuracy of the proposed PVE.

Furthermore, to validate the transient performance of the PVE, the PVE's voltage and current are captured in a DSO for (i) load changes in constant current and voltage regions during the aforementioned uniform irradiance case and (ii) a change in the ratio of partial shading. The PVE's transience for changes in irradiance and temperature are not shown here as they were similar to the PVE's transience for a change in the ratio of partial shading. Figures 18(a) and (b) show the PVE's transience for a load change when the PVE is operating near constant current and constant voltage regions, respectively, whereas Figure 18(c) shows its transient response when the ratio of partial shading is changed from 0.2 to 0.3. As can be seen from Figure 18(a), the proposed PVE settles without any oscillation near the constant current region. Besides, for all the cases, the transience settles within 10 ms which is an acceptable value in comparison with the settling time of 120 ms of commercially available PVE [23].

Thus, the experimental validation shows that the proposed PVE can be implemented using low-cost hardware components which makes it an effective tool for testing new strategies for a solar PV system under both uniform irradiance and partial-shading conditions.

6. Conclusion

In this paper, an ANN-based simplified PVE capable of mimicking a PV panel under uniformly irradiated and partially-shaded conditions is proposed. The proposed PVE linearizes the I-V curve by splitting it into smaller segments with clearly defined boundaries which are determined using an ANN for a given irradiance, temperature, and fraction of partial shading. Furthermore, the problem of oscillations in reference signals in the constant current (voltage) region of operation with voltage (current) control is eliminated by the impedance matching technique without any additional controller. The simulation studies performed in MATLAB/Simulink and the laboratory experiments validate the steady-state accuracy and transient performance of the proposed PVE with a settling time of 10 ms. Also, the accuracy of the proposed PVE can further be improved by increasing the number of segments in the linearization process. Thus, the proposed PVE is well suited for validating the effectiveness of new control strategies under a wide range of variations in temperature, irradiance, and ratio of partial shading. Finally, expanding the degrees-of-freedom during partial-shading operating conditions and generalizing the PVE is considered for future work.

Data Availability

The data used for training the artificial neural network are generated through the solar PV model and are made available to everyone at doi:10.17632/z93gzbptf7.1.

Conflicts of Interest

The authors have no conflict of interest to disclose.

References

[1] A. Hirsch, Y. Parag, and J. Guerrero, "Microgrids: a review of technologies, key drivers, and outstanding issues," *Renewable and Sustainable Energy Reviews*, vol. 90, p. 402, 2018.

[2] Y. Shan, J. Hu, and J. M. Guerrero, "A model predictive power control method for PV and energy storage systems with voltage support capability," *IEEE Transactions on Smart Grid*, vol. 11, no. 2, pp. 1018–1029, 2020.

[3] A. Khan and N. Javaid, "Jaya learning-based optimization for optimal sizing of stand-alone photovoltaic, wind turbine, and battery systems," *Engineering*, vol. 6, no. 7, pp. 812–826, 2020.

[4] Y. Zhang, N. Gatsis, and G. B. Giannakis, "Robust energy management for microgrids with high-penetration renewables," *IEEE Transactions on Sustainable Energy*, vol. 4, no. 4, pp. 944–953, 2013.

[5] S. Shrivastava, B. Subudhi, and S. Das, "Distributed voltage and frequency synchronisation control scheme for islanded inverter-based microgrid," *IET Smart Grid*, vol. 1, no. 2, pp. 48–56, 2018.

[6] J. A. Jiang, T. L. Huang, Y. T. Hsiao, and C. H. Chen, "Maximum power tracking for photovoltaic power systems," *Tamkang J. Sci. Eng.*, vol. 8, no. 2, pp. 147–153, 2005.

[7] Y. Xia, M. Yu, P. Yang, Y. Peng, and W. Wei, "Generation-Storage coordination for islanded DC microgrids dominated by PV generators," *IEEE Transactions on Energy Conversion*, vol. 34, no. 1, pp. 130–138, 2019.

[8] J. P. Ram, H. Manghani, D. S. Pillai, T. S. Babu, M. Miyatake, and N. Rajasekar, "Analysis on solar PV emulators: a review," *Renewable and Sustainable Energy Reviews*, vol. 81, p. 149, 2018.

[9] T. Sudhakar Babu, S. Mohammed Azharuddin, B. Nishant, and N. Rajasekar, "A dynamic photo voltaic emulator using dSPACE controller with high accuracy solar photo voltaic characteristics," *Journal of Renewable and Sustainable Energy*, vol. 8, no. 1, p. 15503, 2016.

[10] I. Moussa and A. Khedher, "Photovoltaic emulator based on PV simulator RT implementation using XSG tools for an FPGA control: theory and experimentation," *International Transactions on Electrical Energy Systems*, vol. 29, no. 8, pp. 1–16, 2019.

[11] R. Ayop and C. W. Tan, "Rapid prototyping of photovoltaic emulator using buck converter based on fast convergence resistance feedback method," *IEEE Transactions on Power Electronics*, vol. 34, no. 9, pp. 8715–8723, 2019.

[12] N. Ullah, F. Nisar, and A. A. Alahmadi, "Closed loop control of photo voltaic emulator using fractional calculus," *IEEE Access*, vol. 8, pp. 28880–28887, 2020.

[13] F. Almonacid, C. Rus, P. J. Pérez, and L. Hontoria, "Estimation of the energy of a PV generator using artificial neural network," *Renewable Energy*, vol. 34, no. 12, pp. 2743–2750, 2009.

[14] N. Kumar, B. Singh, and B. K. Panigrahi, "Framework of gradient descent least squares regression-based NN structure for power quality improvement in PV-integrated low-voltage weak grid system," *IEEE Transactions on Industrial Electronics*, vol. 66, no. 12, pp. 9724–9733, 2019.

[15] B. Singh, N. Kumar, and B. K. Panigrahi, "Steepest descent Laplacian regression based neural network approach for optimal operation of grid supportive solar PV generation," *IEEE Transactions on Circuits and Systems II: Express Briefs*, vol. 68, no. 6, pp. 1947–1951, 2021.

[16] S. I. Sulaiman, T. K. A. Rahman, and R. Musirin, "Prediction of grid-connected photovoltaic system output using evolutionary programming-ANN models," in *In The 8th WSEAS International Conference on Artificial Intelligence, Knowledge Engineering and Data Bases (AIKED'09)*, p. 176+, Cambridge, UK, 2009.

[17] F. Gómez-Castañeda, G. M. Tornez-Xavier, L. M. Flores-Nava, O. Arellano-Cárdenas, and J. A. Moreno-Cadenas, "Photovoltaic panel emulator in FPGA technology using ANFIS approach," in *In 2014 11th International Conference on Electrical Engineering, Computing Science and Automatic Control (CCE)*, pp. 3–8, Ciudad del Carmen, Mexico, 2014.

[18] N. Kumar, B. Singh, B. K. Panigrahi, and L. Xu, "Leaky-least-logarithmic-absolute-difference-based control algorithm and learning-based InC MPPT technique for grid-integrated PV system," *IEEE Transactions on Industrial Electronics*, vol. 66, no. 11, pp. 9003–9012, 2019.

[19] N. Kumar, B. Singh, and B. K. Panigrahi, "LLMLF-based control approach and LPO MPPT technique for improving performance of a multifunctional three-phase two-stage grid integrated PV system," *IEEE Transactions on Sustainable Energy*, vol. 11, no. 1, pp. 371–380, 2020.

[20] N. Kumar, B. Singh, and B. K. Panigrahi, "PNKLMF-based neural network control and learning-based hc mppt technique for multiobjective grid integrated solar pv based distributed generating system," *IEEE Transactions on Industrial Informatics*, vol. 15, no. 6, pp. 3732–3742, 2019.

[21] R. Ayop and C. W. Tan, "An adaptive controller for photovoltaic emulator using artificial neural network," *Indonesian Journal of Electrical Engineering and Computer Science*, vol. 5, no. 3, pp. 556–563, 2017.

[22] U. K. Shinde, S. G. Kadwane, S. P. Gawande, and R. Keshri, "Solar PV emulator for realizing PV characteristics under rapidly varying environmental conditions," in *In 2016 IEEE International Conference on Power Electronics, Drives and Energy Systems (PEDES)*, pp. 1–5, Trivandrum, India, 2017.

[23] H. A. Khawaldeh, M. Al-Soeidat, M. Farhangi, D. D. C. Lu, and L. Li, "Efficiency improvement scheme for PV emulator based on a physical equivalent PV-cell model," *IEEE Access*, vol. 9, pp. 83929–83939, 2021.

[24] I. D. G. Jayawardana, C. N. M. Ho, M. Pokharel, and G. E. Valderrama, "A fast-dynamic control scheme for a power-electronics-based PV emulator," *IEEE Journal of Photovoltaics*, vol. 11, no. 2, pp. 485–495, 2021.

[25] Y.-J. Wang and S.-S. Lin, "Analysis of a partially shaded PV array considering different module connection schemes and effects of bypass diodes," in *In 2011 International Conference & Utility Exhibition on Power and Energy Systems: Issues and Prospects for Asia (ICUE)*, pp. 1–7, Pattaya, Thailand, 2011.

[26] S. R. Wenham, M. A. Green, M. E. Watt, and R. Corkish, *Applied photovoltaics*, Routledge, 2013.

[27] M. G. Villalva, J. R. Gazoli, and E. R. Filho, "Comprehensive approach to modeling and simulation of photovoltaic arrays," *IEEE Transactions on Power Electronics*, vol. 24, no. 5, pp. 1198–1208, 2009.

[28] P. K. Bonthagorla and S. Mikkili, "A novel fixed PV array configuration for harvesting maximum power from shaded

modules by reducing the number of cross-ties," *IEEE Journal of Emerging and Selected Topics in Power Electronics*, vol. 9, no. 2, pp. 2109–2121, 2021.

[29] K.T.S, "V panel: irradiance, temperature, partial shading - IV curves," *Mendeley Data*, 2021.

[30] B. Hauke, *Basic Calculation of a Buck Converter's Power Stage*, 2015.

[31] R. Erickson and D. Maksimovic, *Fundamentals of Power Electronics*, Kluwer Academic Publishers, 2nd edition, 2004.